small structures
www.small-structures.com

Vancomycin-Modified DNA Origami Nanostructures for Targeting Bacterial Pathogens

Özge Coşkuner Leineweber, Bhanu K. Pothineni, Nils Schumann, Ulrike Hofmann, Christin Möser, David M. Smith, Guido Grundmeier, Yixin Zhang, and Adrian Keller**

The specific binding of DNA origami nanostructures (DONs) to bacteria is an important prerequisite for their application in pathogen targeting and antimicrobial drug delivery. So far, targeting bacteria with DONs has been achieved exclusively via aptamers, which suffer from drawbacks such as sensitivity toward environmental conditions and reduced binding after immobilization or conjugation. Here, an alternative approach is presented based on the modification of DONs with the cell wall-binding glycopeptide antibiotic vancomycin. Using strain-promoted azide-alkyne cycloaddition, azide-modified vancomycin is conjugated to selected staple strands and subsequently incorporated into 2D DON triangles. The resulting constructs show specific binding to the Gram-positive species *Bacillus subtilis* (*B. subtilis*) and *Staphylococcus capitis* (*S. capitis*), and remarkably, to Gram-negative *Escherichia coli* (*E. coli*), but no antimicrobial activity at vancomycin concentrations up to at least 2.91 μM. For *B. subtilis* and *E. coli*, DONs with vancomycin modifications on both sides exhibit better binding than DONs modified on only one side. However, both variants bind equally well to *S. capitis*. These results demonstrate the great potential of small molecule drug compounds for the robust, broad-spectrum targeting of bacteria with DONs. Targeting a ubiquitous cell wall component of most pathogenic bacteria, vancomycin-modified DONs have many potential applications in the prevention and treatment of nosocomial infections.

1. Introduction

The rapid, worldwide spreading of antimicrobial resistance (AMR) represents a grave threat to humanity.[1] At the same time, the number of new antibiotics reaching the clinic each year has dropped to dangerously low levels over the last decades[2–4] and alternative strategies for the treatment of bacterial infections are urgently needed.[5] In this regard, nanomaterials are showing great potential, both as new antimicrobial agents with novel mechanisms of action and as delivery vehicles for established antibiotics.[6–9] While most works in this field have focused on inorganic, polymer, or lipid nanoparticles, DNA nanostructures are currently receiving a lot of attention in this context as well.[10] DNA origami nanostructures (DONs)[11] are particularly promising drug delivery vehicles because they are nontoxic in vivo,[12,13] can be mass-produced at low costs by established biotechnological methods,[14] and are compatible with automated robotic purification.[15] Being fully biodegradable, they have a limited lifetime in vivo but their stability in physiological environments can be enhanced and even tailored to meet specific application requirements, for instance by rational design choices[16,17] or the application of protective coatings.[18,19] Furthermore, DONs can be loaded with numerous therapeutic cargos such as small molecules,[20–22] enzymes,[23] and nucleic acids[24] via intercalation,[21] groove binding,[20,25] covalent coupling,[22] and protein-ligand binding.[23] While the vast majority of previous works have focused on applications in cancer therapy,[26,27] recent studies have also demonstrated successful DON-based delivery of antimicrobial agents to bacteria both in

Ö. Coşkuner Leineweber, B. K. Pothineni,[+] G. Grundmeier, A. Keller
Technical and Macromolecular Chemistry
Paderborn University
Warburger Str. 100, 33098 Paderborn, Germany
E-mail: adrian.keller@uni-paderborn.de

The ORCID identification number(s) for the author(s) of this article can be found under https://doi.org/10.1002/sstr.202500246.

[+]Present address: Programmable Biomaterials Laboratory, Institute of Materials, School of Engineering, Ecole Polytechnique Federale de Lausanne, Lausanne 1015, Switzerland

DOI: 10.1002/sstr.202500246

N. Schumann, U. Hofmann, Y. Zhang
B CUBE – Center for Molecular Bioengineering
Technische Universität Dresden
Tatzberg 41, 01307 Dresden, Germany
E-mail: yixin.zhang1@tu-dresden.de

C. Möser, D. M. Smith
DNA Nanodevices Unit, Department Diagnostics
Fraunhofer Institute for Cell Therapy and Immunology IZI
04103 Leipzig, Germany

vitro[23,28] and in vivo.[28] Most importantly in this field of application, DONs can be equipped with multiple independent mechanisms of action by precise loading with multiple copies of diverse antimicrobial elements, such as enzymes,[23] DNAzymes,[28] photosensitizers,[29] and regular antibiotics.[28] Additionally, targeting elements can be introduced in a similar manner, allowing the DONs to specifically bind to the target pathogen and facilitate its selective inhibition.[23,28] In virtually all previous studies, this was achieved via the incorporation of aptamers that recognize specific components of the bacterial cell surface.[23,28,30]

Equipping DONs with aptamers can be achieved via a simple extension of selected staple strands, which makes it a straightforward and frequently used approach.[31] As targeting entities, however, aptamers have drawbacks. Most importantly, efficient target binding relies on the aptamer adopting a specific 3D topology, which is very sensitive toward many environmental conditions[32] such as pH, temperature, and the presence and concentration of certain ions.[33,34] Furthermore, surface immobilization[35,36] and chemical conjugation[37,38] of aptamers may strongly affect their folding and target binding performance and even result in a complete loss of functionality.[38] Bacteria-targeting aptamers are additionally often not only specific for certain species but also exhibit strain-dependent binding.[39] To enable the clinical application of antimicrobial DONs, more robust strategies for the efficient targeting of bacterial cells are required. In this work, we explore the ability of DNA-conjugated vancomycin to facilitate DNA origami binding to Gram-positive and Gram-negative bacteria.

Vancomycin is a glycopeptide antibiotic that binds to the terminal D-Ala-D-Ala stem peptides of the peptidoglycans that make up the Gram-positive cell wall (**Figure 1**).[40] The drug blocks the cross-linking of the cell wall by transpeptidase enzymes and thereby inhibits bacterial growth. Vancomycin binds to its target via five H-bonds, with a dissociation constant $K_d \approx 1$ μM. However, binding can be increased dramatically in multivalent binding complexes.[41] Therefore, immobilization of multiple vancomycin molecules on the surfaces of nanoparticles is frequently used for the efficient targeting of bacterial cells for purposes of bacteria detection, capture, and concentration.[42–46] The strongly increased binding affinity of multimeric vancomycin-nanoparticle conjugates in general also enables their efficient binding to vancomycin-resistant strains, in which the D-Ala-D-Ala target peptides are replaced by D-Ala-D-Lac.[8] Most interestingly, such vancomycin-conjugated nanoparticles often also bind to Gram-negative bacteria[42,45,46] even though monomeric vancomycin is only active against Gram-positive species.[40] DNA-conjugated vancomycin may thus serve as a versatile tool in the synthesis of broad-spectrum DONs with the ability to bind to a wide range of bacterial pathogens.

2. Results and Discussion

Selected amino-modified staple strands of the DON triangle were modified with dibenzocyclooctyne-*N*-hydroxysuccinimidyl (DBCO-NHS) ester and azide vancomycin was conjugated to the resulting DBCO-DNA constructs via strain-promoted azide-alkyne cycloaddition (SPAAC, see Figure 1 and **2**a). To provide sufficient structural flexibility for target binding, an additional T_6 spacer was introduced

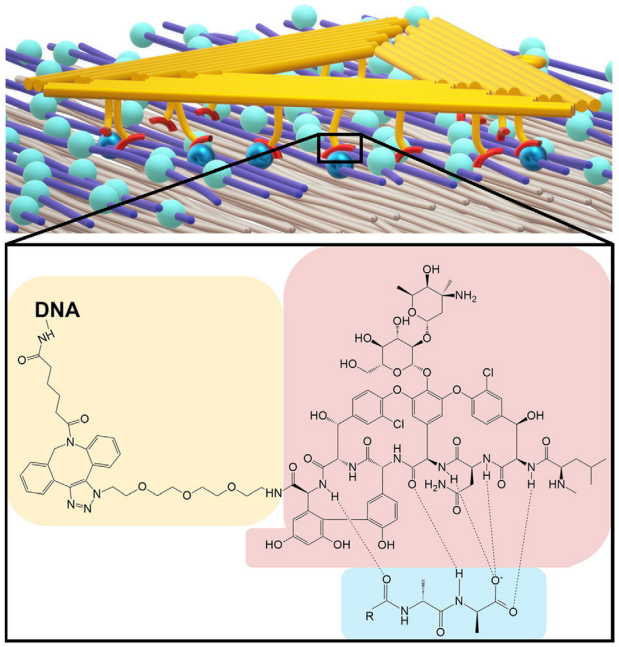

Figure 1. Schematic representation of a DON triangle bound to a Gram-positive bacterial cell wall via vancomycin-conjugated staple overhangs displayed on the DON. In the molecular structure of the binding complex, vancomycin is indicated in red, the linker in yellow, and the D-Ala-D-Ala target peptide in blue.

to the staple strands. DBCO modification of the amino-modified staples was verified by their UV absorption at 310 nm (see Figure S1–S3, Supporting Information). Figure 2b shows the polyacrylamide gel electrophoresis (PAGE) analysis of three selected staple strands before and after the DBCO modification and azide vancomycin conjugation steps. In all three examples, notably reduced electrophoretic mobility is observed for the vancomycin–staple (V–S) conjugates. Quantitative analysis of the PAGE gels revealed conjugation yields ranging from 60 to 99% (see Figure S5, Supporting Information), with an average yield of 85 ± 11%. Successful vancomycin-staple conjugation was also verified by high performance liquid chromatography-mass spectrometry (HPLC-MS) (see Figure S6–S9, Supporting Information).

The V–S conjugates were combined with nonmodified staples and scaffold and assembled into triangular DONs presenting nominally 18 vancomycin molecules either on just one side (V18–DON) or on both sides (V36–DON, see Figure 2a and S21, and Table S1, Supporting Information). Successful assembly was verified by atomic force microscopy (AFM, see Figure 2c). Note that the vancomycin modifications are too small to be resolved by AFM. Rather, we attempted to verify V–S incorporation by agarose gel electrophoresis, which indeed showed different electrophoretic mobilities of the different DNA origami constructs. While these shifts were highly reproducible, the V18–DON and bare DON consistently showed the highest and lowest mobility, respectively, with the V36–DON having an intermediate mobility (see Figure S10, Supporting Information). This is probably related to vancomycin attachment increasing not only the mass and hydrodynamic radius of the DONs but also adding

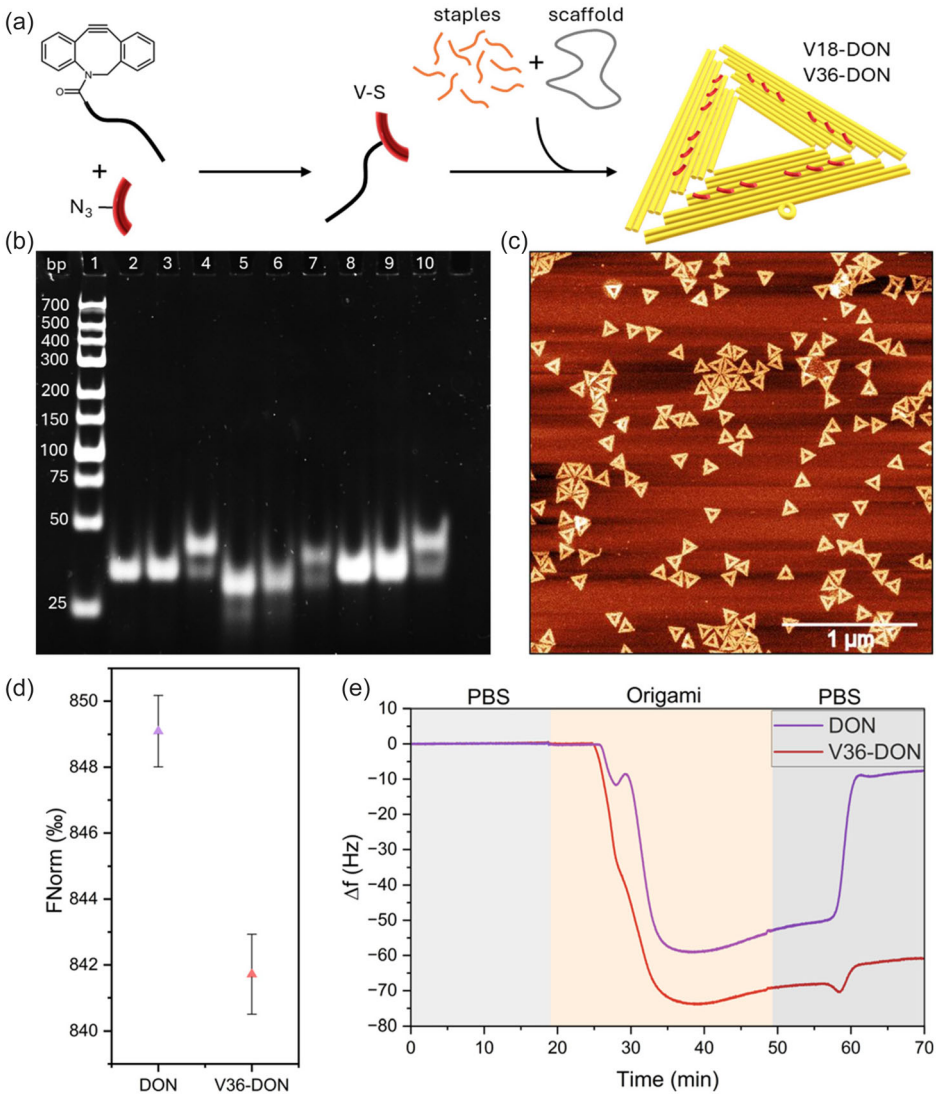

Figure 2. a) Synthesis scheme. Azide-modified vancomycin (red) is conjugated to DBCO-modified staples (black). The resulting V–S conjugates are then mixed with nonmodified staples at equimolar concentrations and scaffold to produce DON triangles with 18 vancomycin molecules presented either on just one side (V18–DON) or on both sides (V36–DON). b) Native PAGE image of amino-modified (2, 5, and 8), DBCO-modified (3, 6, and 9), and vancomycin-conjugated (4, 7, and 10) staple strands t-4s7f (2–4), t-4s17f (5–7), and t-4s27f (8–10), respectively. Lane 1 shows a 700 bp low-range DNA ladder. See Figure S4 for the complete dataset. c) AFM image of V36–DONs on mica. d) Thermophoretic mobility assay of V36–DONs and bare DONs. Experiments were performed in triplicate ($n = 3$) and are presented as mean values with the standard deviation as error bars. Differences are statistically significant with $p < 0.05$ as determined by a two-sided t-test. See Figure S11 for time-dependent MST signals. e) Adsorption and desorption of V36–DONs and bare DONs on D-Ala-D-Ala peptides immobilized on QCM-D sensors monitored by the change in resonance frequency Δf (5th overtone, see Figure S13, Supporting Information, for the complete datasets).

positive charges. In addition, large numbers of modifications can result in pronounced changes in the 3D shape of the DON.[47] All these factors have diverse effects on DON migration through the gel. We also used microscale thermophoresis (MST) to verify vancomycin incorporation as another independent method, because the thermodiffusion of biomolecules is affected by their hydrodynamic environment.[48] As shown in Figure 2d, different thermophoretic mobilities are observed for V36–DON and the bare DON, confirming successful vancomycin incorporation. Unfortunately, this method does not allow us to quantify the incorporation yields of the V–S conjugates into the DON. Based on our extensive experience with small molecule staple modifications of DONs,[49–55] however, we assume an average incorporation yield >85% for modified staples. A computational simulation using a combined conjugation and incorporation yield of 72% revealed that 57% of V36-DONs carry at least 26 vancomycin modifications (see Figure S12, Supporting Information).

Specific binding of V36–DONs to the target D-Ala-D-Ala-containing peptides was verified using quartz crystal microbalance with dissipation monitoring (QCM-D). For this, a synthetic

peptide sequence corresponding to the stem peptide of enterococcal cell walls[56] was immobilized on the gold electrodes of QCM-D sensors with the help of an additional N-terminal cysteine (Cys-Gly-Gly-Gly-L-Ala-D-Glu-L-Lys-D-Ala-D-Ala-COOH). Binding of V36–DONs and bare DONs to the immobilized peptides was investigated by monitoring the change in resonance frequency Δf, which is a measure of the adsorbed mass.[57] As shown in Figure 2e, injection of the sample solution results in a decrease in Δf for both DONs and V36–DONs, indicating adsorption of both DON variants on the electrode surface. However, the decrease in Δf is stronger for V36–DONs than for bare DONs, which we attribute to the specific binding of the displayed vancomycin molecules on DONs to the immobilized peptides. More importantly, this specific binding is responsible for the different behaviors of the adsorbed nanostructures upon washing with PBS buffer. For bare DONs, washing leads to notable desorption, so that the Δf trace is rapidly restored to almost 0. For V36–DONs, however, desorption is greatly reduced with Δf remaining at about −60 Hz, which proves a stronger attachment of V36–DONs compared to bare DONs. These results thus demonstrate that vancomycin is able to bind to its target peptide when displayed on the surface of DONs.

Next, we quantitatively assessed the binding of the vancomycin-presenting DONs to the Gram-positive model bacterium *Bacillus subtilis* (*B. subtilis*) using an enzyme-linked oligonucleotide assay (ELONA).[30] For this, the DONs were equipped with six biotinylated staple overhangs at their edges (see Figure S21 and table S2, Supporting Information) to facilitate binding of HRP-conjugated streptavidin. Note that this requires the accessibility of the biotin modifications of the DONs after binding to the bacteria, so that only surface-bound DONs can be detected, but not internalized ones. As can be seen in **Figure 3**a, no binding of bare DONs to *B. subtilis* is observed. In contrast, V18–DON binding yields an absorbance signal that is more than twice as high as that of the bare DON. Presenting vancomycin not just on one but on both sides of the DON (i.e., V36–DON) results in a further enhancement of binding by another 48% compared to V18–DON. This proves not only successful targeting but also demonstrates the benefits of presenting vancomycin on both sides of the DON. The observation that the increase in absorbance has roughly the same magnitude when comparing V18–DONs to bare DONs and V36–DONs to V18–DONs suggests that the initial interaction with the cell surface is facilitated by nonspecific adsorption, which is largely independent of the displayed vancomycin molecules, as already observed in the QCM-D experiments shown in Figure 2e. Vancomycin-presenting DONs, however, are bound more tightly and thus less likely to desorb during washing (see Figure 2e), indicating that they adsorb with their vancomycin modifications pointing toward the cell wall. For V18–DON, the probability of this happening is about 50%, whereas for V36–DON with both sides displaying the same number of vancomycin modifications, the probability increases to 100%, thus leading to a doubling in the signal of the bound DONs.

A frequently observed issue in aptamer-mediated binding is the strong dependence of the binding affinity on the ionic composition of the surrounding medium.[33,34] For example, Siddiqui et al. studied the effect of the Mg^{2+} concentration on the binding of four aptamers specific for *Escherichia coli* (*E. coli*) O157:H7.[58] Two of the four aptamers under investigation showed Mg^{2+}-dependent target binding, with maximum binding observed at a Mg^{2+} concentration of 5 mM. Higher as well as lower concentrations led to a pronounced reduction in target binding. Similarly, the Protein A-specific aptamer used by Ahmadi et al. to facilitate DON binding to *Staphylococcus aureus* (*S. aureus*) cells required the presence of Mg^{2+} in mM concentrations for efficient target binding.[30] Furthermore, this particular aptamer had to be heat-activated at 95 °C in 10 mM Mg^{2+} before it could be hybridized to the DON. Since the ELONA experiments described above were conducted in PBS supplemented with 10 mM Mg^{2+}, we also investigated binding of V36–DON to *B. subtilis* in Mg^{2+}-free PBS (see Figure 3b). Under those conditions, binding is reduced by about 30%, which can be attributed to the divalent cation's ability to promote nonspecific adsorption of the negatively charged DONs on the cell surface,[59] which is also negatively charged.[60] Nevertheless, this reduction in binding is markedly smaller than that observed in the aptamer studies mentioned above (70 to 85% reduction for the two *E. coli* aptamers[58] and 92% reduction for the *S. aureus* aptamer),[30] showcasing the environmental robustness of the small molecule binder.

It has been shown before that the multimeric presentation of vancomycin on nanoparticle surfaces may result in enhanced antimicrobial activity.[8] Therefore, we also tested the antimicrobial effect of V36–DON on *B. subtilis* using broth microdilution (Figure 3c). For the small molecule drug vancomycin (V), a minimum inhibitory concentration (MIC) of 1.45 μM is determined, corresponding to 2.1 $\mu g\,mL^{-1}$. This MIC is higher than those reported in literature,[61,62] which may be due to the presence of $MgCl_2$ in the medium that was added to ensure DON stability. V36–DON shows a lower antimicrobial activity with a MIC >2.91 μM vancomycin against *B. subtilis* (Figure 3c). This was confirmed by scanning electron microscopy (SEM), which revealed many dead bacteria after exposure to free vancomycin, whereas only live bacteria were observed after incubation with V36–DON at the same vancomycin concentration (Figure 3d and S16–S18, Supporting Information). In order to verify that this is not caused by the conjugation to the staple strands, a single V–S conjugate was also tested against *B. subtilis* at 2.91 μM, showing full growth inhibition (Figure 3c). Therefore, we assume that the reduced activity of V36–DON is caused by the large size of the DONs (≈120 nm edge length), which are unable to penetrate the *B. subtilis* cell wall but rather adsorb on the cell surface in a flat geometry. This means that the vancomycin modifications bind only to and inhibit the crosslinking of the outermost D-Ala-D-Ala peptides, which has no notable effect on the integrity of the total cell wall with an average thickness of more than 30 nm.[63] In addition, simulations suggest that the DON triangles adopt a cup-like shape in bulk solution,[17,64] which is consistent with experimental observations.[52,65,66] In our system, such a distorted shape may result in a topological mismatch between DON and the cell surface, allowing only a few vancomycin molecules to effectively interact with the cell wall and inhibit crosslinking.

Since *B. subtilis* is a model bacterium with no clinical relevance, we next evaluated vancomycin-mediated binding of DONs to a clinically relevant, coagulase-negative *Staphylococcus*. *Staphylococcus capitis* (*S. capitis*) is an emerging Gram-positive AMR pathogen known to cause bloodstream infections, implant-associated

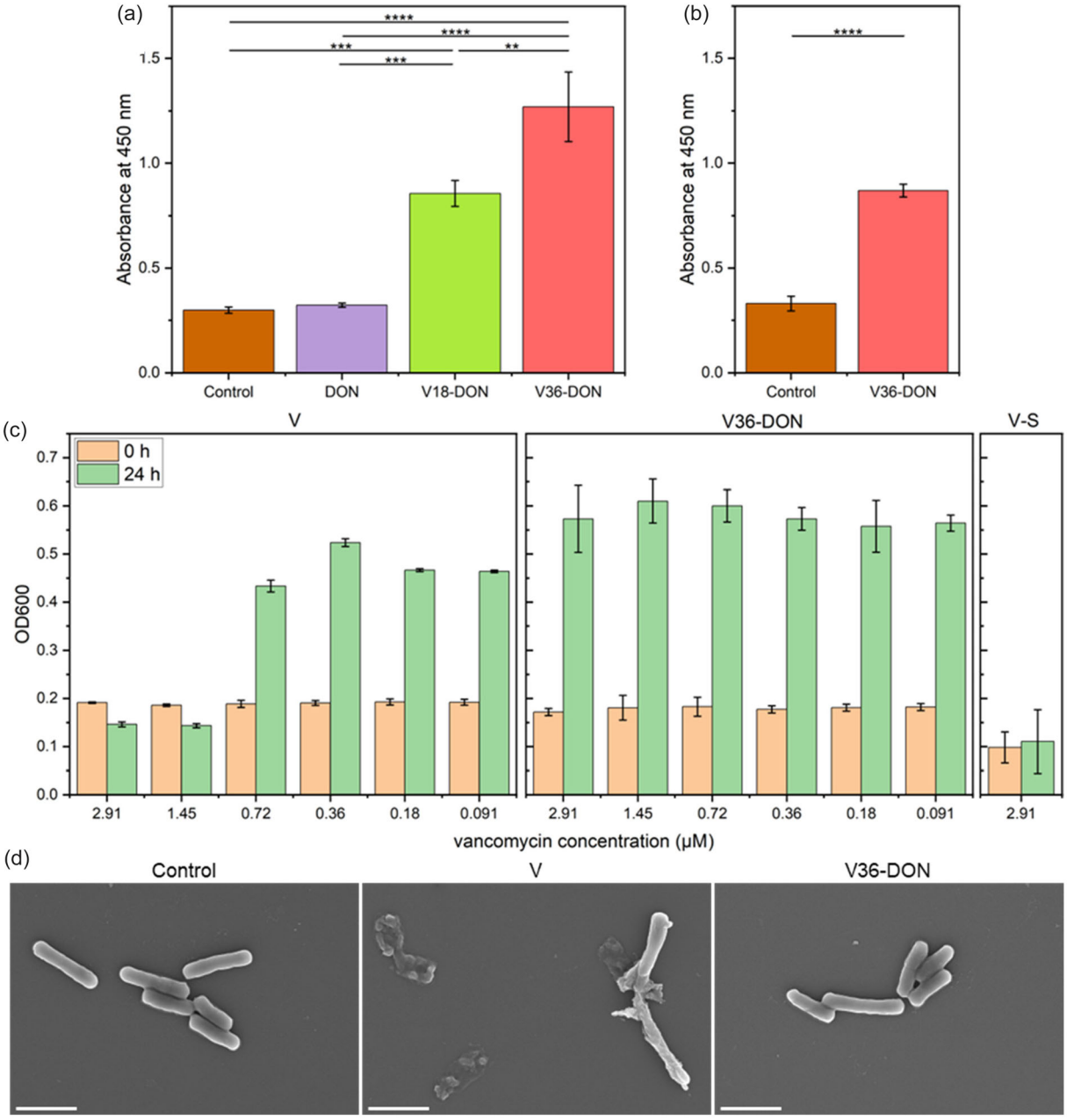

Figure 3. a,b) ELONA results of (a) bare and vancomycin-presenting DONs (46 nM) binding to *B. subtilis* in Mg^{2+}-supplemented PBS and (b) vancomycin-presenting DONs (46 nM) binding to *B. subtilis* in Mg^{2+}-free PBS. Experiments were performed in triplicate ($n = 3$) and are presented as mean values with the standard deviation as error bars. Statistical significances were calculated using a one-way ANOVA and are indicated as * ($p < 0.05$), ** ($p < 0.01$), *** ($p < 0.001$), and **** ($p < 0.0001$). c) Effect of the small molecule drug vancomycin (V), V36–DON, and a single V–S conjugate on the growth of *B. subtilis* assessed by broth microdilution. Bacterial growth is evaluated after 0 and 24 h of incubation via the optical density measurement at 600 nm (OD600). Experiments were performed in triplicate ($n = 3$) and are presented as mean values with the standard deviation as error bars. See Figure S15 for the controls. d) Scanning Electron Microscopy(SEM) images of *B. subtilis* after exposure to V and V36–DON, respectively, at a vancomycin concentration of 2.91 μM. Scale bars are 2 μm. For larger images, see Figure S16–S18, Supporting Information.

infections, and other nosocomial infections.[67] The ELONA results in **Figure 4** reveal significant binding of bare DONs to the surface of *S. capitis*. Since no binding of bare DONs is observed for *B. subtilis* (Figure 3a), this demonstrates the relevance of species-dependent factors in nonspecific adsorption. In particular, while both *S. capitis* and *B. subtilis* have negatively charged cell surfaces, the zeta potential of *B. subtilis* is markedly more negative (−15 to −55 mV, depending on strain)[60] than that of *Staphylococcus* species (about −5 mV).[68] This will result in weaker electrostatic repulsion between the DONs and the *S. capitis* cell surface and thus stronger

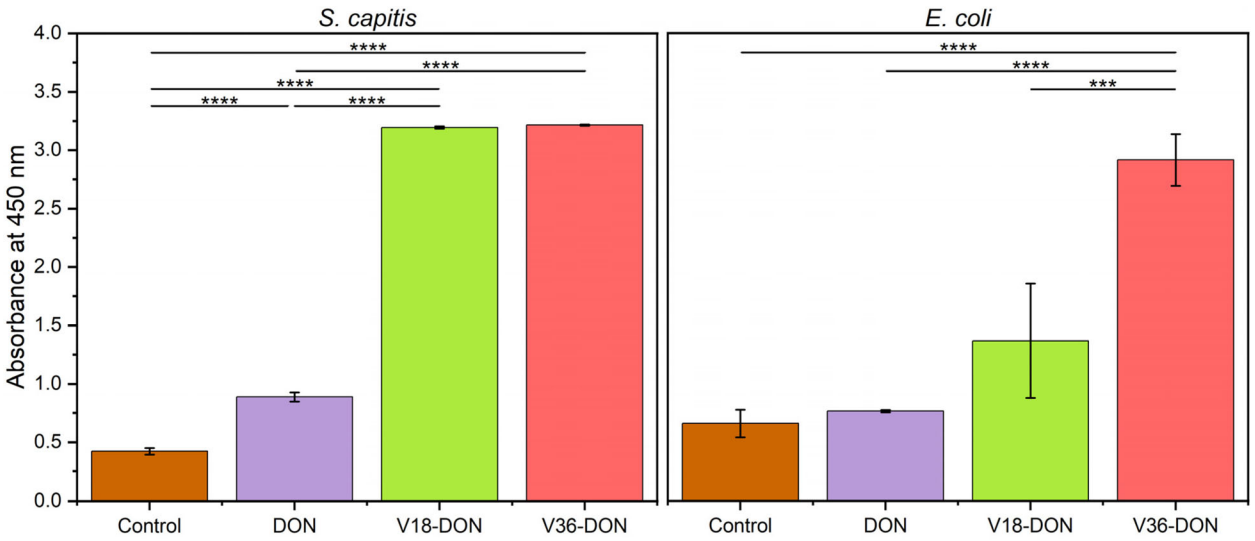

Figure 4. ELONA results of bare and vancomycin-presenting DONs (46 nM) binding to *S. capitis* (left) and *E. coli* (right). Experiments were performed in triplicate ($n = 3$) and are presented as mean values with the standard deviation as error bars. Statistical significances were calculated using a one-way ANOVA and are indicated as * ($p < 0.05$), ** ($p < 0.01$), *** ($p < 0.001$), and **** ($p < 0.0001$).

nonspecific adsorption. This effect might also contribute to the stronger binding of V18–DON, which is increased threefold compared to bare DONs. Surprisingly, the binding of V18–DON to *S. capitis* is virtually identical to that of V36–DON, which is in stark contrast to the observations for *B. subtilis* in Figure 3a. While this may again be caused by the only weakly negative zeta potential resulting in saturated DON coverage on the cell surface, it might also indicate that the DONs are sinking deeper into the cell wall environment, so that V18–DONs are able to bind to their target peptides even when their vancomycin modifications face away from the cell surface. Nevertheless, no effect of V36–DON on the growth of *S. capitis* is observed at this concentration (see Figure S19, Supporting Information).

In order to assess whether the vancomycin-modified DONs are also able to bind to Gram-negative bacteria, further ELONA experiments were performed using *E. coli* as the target bacterium, which is a common, clinically relevant bacterial pathogen[69] that can cause diarrhea, urinary tract infections, and meningitis.[70] In 2019, AMR *E. coli* infections were associated with more than 750 000 deaths worldwide, making it the world's leading AMR pathogen.[71] As in the case of *B. subtilis*, adsorption of bare DONs to the cell surface was found to be low (see Figure 3), which is in line with the zeta potential of this *E. coli* strain (about −20 mV)[72] being comparable to that of *B. subtilis*. While V18–DON on average shows strongly enhanced binding, the large variation between replicates renders the observed increase less significant. However, displaying vancomycin on both sides of the DON results in a more than fourfold increase in absorbance compared to the control. This strong binding is quite remarkable considering that Gram-negative bacteria are intrinsically resistant toward vancomycin because their outer membranes restrict access to the cell wall.[73] Nevertheless, V36–DON binding did not affect bacterial growth (Figure S20, Supporting Information). In the absence of any biotin modifications, a low ELONA signal is detected for the binding of V36–DON (see Figure S14, Supporting Information), verifying that the strong increase in absorbance observed for this construct is indeed caused by enhanced binding to the bacteria and not by interactions between the vancomycin modifications and the HRP-conjugated streptavidin. The large differences in binding of V36–DON and V18–DON may point toward differences in their interactions with the *E. coli* cell surfaces compared to those of the Gram-positive bacteria. On the *E. coli* surface, for instance, the initial adsorption of V18–DONs may be biased in such a way that they adsorb preferentially with the nonmodified side, thus reducing the effective binding with the vancomycin-modified side kinetically. For V36–DONs with modifications on both sides, any initial nonspecific interaction will be followed by the specific multivalent interaction between the displayed vancomycin modifications and the cell surface.

3. Conclusion

In summary, we have synthesized 2D DON triangles that present 18 or 36 vancomycin molecules on their surfaces. This was achieved by conjugating azide-modified vancomycin to selected staple strands via click chemistry. The vancomycin-presenting DONs showed improved binding to surface-immobilized synthetic D-Ala-D-Ala peptides, as well as to Gram-positive *B. subtilis* and *S. capitis* and Gram-negative *E. coli* cells. For *B. subtilis* and *E. coli*, DONs carrying 18 vancomycin modifications on each of their two sides showed improved binding compared to DONs with 18 vancomycin modifications on only one side. In contrast, both DON variants were found to bind equally well to *S. capitis*. Furthermore, our experiments suggest species-dependent differences in the interaction of DONs with the cell surfaces of *B. subtilis*, *S. capitis*, and *E. coli*, with electrostatic repulsion playing a particularly important role.

Our results demonstrate the great potential of vancomycin conjugates to facilitate the robust, broad-spectrum targeting of Gram-positive and Gram-negative bacteria. Their molecular target is a ubiquitous component of the cell walls of most pathogenic bacteria, including the ESKAPE pathogens *Enterococcus faecium, S. aureus, Klebsiella pneumoniae, Acinetobacter baumannii, Pseudomonas aeruginosa,* and *Enterobacter spp,* thus rendering vancomycin-modified DONs widely applicable for the detection and prevention of nosocomial infections. In contrast to aptamers, the vancomycin modifications introduced here do not require the presence of specific ions and are not affected in their target binding capability by DNA conjugation and immobilization on the DON surfaces. Furthermore, due to the covalent conjugation of vancomycin to the staple strands of the DONs, loss of targeting capability is less likely than in cases where the aptamers or other targeting moieties were immobilized via sticky-end hybridization.[28,30] By replacing aptamers with a small molecule binder, the most vulnerable component in the targeting system has thus been eliminated. While this leaves the DONs themselves as the weakest point, they can efficiently be stabilized under physiologically relevant conditions using a variety of methods.[74] This paves the way toward clinical applications of vancomycin-presenting DONs.

4. Experimental Section

Azide vancomycin synthesis: 100 mg of vancomycin (Sigma-Aldrich) in 1 mL DMSO was added to 26.2 mg of 2-(1*H*-Benzotriazol-1-yl)-1,1,3,3-tetramethyluronium-hexafluorophosphat (HBTU, 1 eq.) in 0.3 mL DMSO in a glass vial with a magnetic stirrer. After 20 min, 20 µL NH_2-PEG(3)-N_3 (1.5 eq.) in 200 µL DMSO and 92 µL DIPEA (7.5 eq.) were added to the activated vancomycin. After reaction overnight, the product was purified by reverse phase HPLC (Waters) with a C18 column and the molecular weight was confirmed by liquid chromatography-MS (LC-MS) (Waters) ($[M+H]^+$: 1650.5 calculated, 1649.9 measured).

Vancomycin-staple conjugation: For vancomycin presentation on the DONs, 36 staple strands were selected. The nonpurified staples with 3′ amino modifications (see Figure S21 and table S1, Supporting Information) were purchased from Metabion International. The staples were resuspended in HPLC-grade water (Carl Roth) and purified by ethanol precipitation. The amino-modified staples were then modified with DBCO-NHS ester. For this, the amino-modified staples were incubated overnight at room temperature in PBS (pH 7.4, Thermo Scientific) with a 100-fold molar excess of DBCO-NHS ester (Lumiprobe) dissolved in DMSO (≥99.5%, Carl Roth) at 10 mM. Afterward, the DBCO-modified staples were purified from excess DBCO-NHS ester by ethanol precipitation. The presence of the DBCO moiety on the staples was verified with UV/vis absorption (Nanophotometer P330, Implen) at 310 nm (see Figure S1–S3, Supporting Information).[75–77] The DBCO-modified staples were then incubated overnight at room temperature in PBS (pH 7.4) with a 20-fold molar excess of azide vancomycin (1 mg mL^{-1}).

Native polyacrylamide gel electrophoresis (PAGE): To confirm successful vancomycin-staple conjugation, 8% v/v polyacrylamide gel was prepared by mixing 1.4 mL acrylamide-bisacrylamide (29:1 (40%), Sigma-Aldrich), 1.4 mL 5x TBE (Carl-Roth), 4.1 mL deionized water (VWR), 70 µL 10% ammonium persulfate (APS, ≥98%, Sigma-Aldrich) and 7 µL N,N,N′, N′-tetramethylethylendiamin (TEMED, ≥99.0%, Thermo Scientific). The samples were prepared at a concentration of 2 µM in 1x TBE supplemented with 6x Orange DNA loading dye (Thermo Fisher). During PAGE analysis, 5 µL of each sample and GeneRuler low range DNA ladder (Thermo Fisher) were run at 150 V for 2 h in 1x TBE buffer using a vertical gel electrophoresis system (VWR shiroGel Mini). After PAGE, the gels were stained in 1x TBE with SYBR gold nucleic acid gel stain (Thermo Fisher) at a final concentration of 1x and visualized using a GelJet Imager (Intas Science Imaging Instruments) and software Intas GDS Touch 2. The gel bands were quantified with GelAnalyzer 23.1.1 (available at www.gelanalyzer.com) by Istvan Lazar Jr., Ph.D. and Istvan Lazar Sr., Ph.D., CSc.

High-performance liquid chromatography (HPLC) and mass spectrometry (MS) analysis of DNA conjugates: Selected vancomycin-staple conjugation products were analyzed by ultra-high performance liquid chromatography (monitored at wavelength 260 nm) coupled with electrospray ionization-mass spectrometry (UPLC–ESI–MS, Waters).

DNA origami folding: For DNA origami folding, 30 µL M13mp18 scaffold (Bayou Biolabs), 60 µL of an equimolar mixture of 172 nonmodified staples (Eurofins), 20 µL of 10x TAE (Carl Roth) with 100 mM $MgCl_2$ (Carl Roth), and 1 µL of each of the selected 36 staples with or without vancomycin modifications were mixed and 54 µL of HPLC-grade water were added to reach a final volume of 200 µL, with final concentrations of 15 nM scaffold and 150 nM per staple. The mixture was heated to 80 °C in a thermocycler (Ristretto, VWR) and cooled down gradually to room temperature over a time span of 90 min as described previously.[78] The assembled nanostructures were filtered using 100 kDa Amicon Ultra spin filters (Millipore) to remove unbound staples. The concentration of the synthesized DNA origami triangles was measured using UV/vis absorption (Nanophotometer P330, Implen).

Atomic force microscopy (AFM): The integrity of the synthesized V36–DONs was verified by AFM. 100 µL of 1 nM V36–DONs in 1x TAE supplemented with 10 mM $MgCl_2$ was deposited on a freshly cleaved mica surface and incubated for 1 min, after which the sample was carefully washed with 7 mL of HPLC-grade water and dried in a stream of argon. The samples were imaged in the dry state using a Dimension ICON AFM (Bruker) in ScanAsyst Peak-Force Tapping mode with ScanAsyst Air cantilevers (Bruker). The images were flattened and processed using Gwyddion.[79]

Agarose gel electrophoresis: Agarose gel electrophoresis was performed to confirm successful vancomycin-modification of the DONs. A 5 mm, 0.7% w/v agarose gel was prepared by dissolving 0.7 g agarose powder (Electran, VWR) in 90 mL 1x TAE (Carl Roth) by heating until a clear solution was obtained and adding 1 mL of deionized water to compensate for evaporation. The solution was left to cool to ≈50 to 60 °C, after which 10 mL of 1x TAE containing 110 mM $MgCl_2$ and 2.5 µL SYBR gold nucleic acid gel stain at a final concentration of 2.5x (Thermo Fisher) was added. The samples were prepared at a concentration of 5 nM in 1x TAE supplemented with 11 mM $MgCl_2$ and 6x Orange DNA Loading Dye (Thermo Fisher). 10 µL samples of V18–DONs, V36–DONs, and bare DONs were loaded into the gel and electrophoresis was performed using a horizontal gel electrophoresis system (VWR PerfectBlue Mini M) at 60 V for 3 h in 1x TAE containing 11 mM $MgCl_2$ running buffer. Afterward, the gel was visualized using a GelJet Imager (Intas Science Imaging Instruments) and software Intas GDS Touch 2.

Microscale thermophoresis (MST): For MST analysis, V36–DONs and bare DONs were labeled with a fluorophore via incorporation of a Cy5-labeled staple (Cy5-T_4-t-2s1g, 5′-Cy5-TTT TAA AAC AAA ATT AAT TAA ATG GAA ACA GTA CAT TAG TGA AT-3′, HPLC-purified, Metabion International). MST was performed using a NanoTemper Monolith NT.Automated (NanoTemper Technologies). Samples were prepared in polystyrene 384-well plates (Corning) and then loaded into Monolith NT.Automated capillary chips. MST was carried out at DON concentrations of 0.25 nM in PBST (PBS + 0.05% Tween 20) buffer.

Peptide synthesis: The peptide Cys-Gly-Gly-Gly-L-Ala-D-Glu-L-Lys-D-Ala-D-Ala-COOH was synthesized using standard Fmoc solid-phase peptide synthesis on Fmoc-D-Ala-Wang resin with 2-(1H-benzotriazol-1-yl)-1,1,3,3-tetramethyluronoium hexafluorophosphate (HBTU) as activation reagent on an automated solid-phase peptide synthesizer (ResPep SL, Intavis). For achieving high yield, each amino acid was coupled twice with five times excess each, and all unreacted amino groups were capped with acetic anhydride. The peptide was cleaved from the resin with TFA/TIS/water/DTT (90v/v:5v/v:2.5v/v:2.5(m/v)) for 1.5 h. The product was precipitated and washed with ice-cold diethyl ether. After HPLC purification with a reverse phase C18 HPLC column, the molecular weight was confirmed by LC-MS ($[M+H]^+$: 763.84 calculated, 763.28 measured).

Quartz crystal microbalance with dissipation monitoring (QCM-D): The flow cells and inlet pipes of the QCM-D system (E4, Biolin Scientific) were

incubated in 2% Hellmanex (Hellma) for 2 h, rinsed with HPLC-grade water, and dried in a stream of argon. 5 MHz AT-cut gold-coated QCM sensors (14 mm Cr/Au, Quartz Pro, Sweden) were cleaned in RCA1 solution (1:1:5 in volume 35% NH_4OH, 25% H_2O_2, H_2O). 0.28 mM peptide was dissolved in 10 mL PBS and the cleaned crystals were incubated in the peptide solution for 24 h. Afterward, the crystals were rinsed in HPLC-grade water, dried in a stream of argon, and mounted in the QCM-D flow cells. A flow rate of 10 µL min^{-1} was used. Initially, a constant baseline was established using PBS for 19 min, after which DONs with and without vancomycin modifications in 1x TAE supplemented with 10 mM $MgCl_2$ at a concentration of 5 nM were injected into the flow cells until a stable plateau in the Δf curves was obtained (30 min). The flow cells were then flushed with PBS to remove unbound and loosely bound DONs from the peptide monolayer (20 min) until a new plateau was reached.

Cultivation of bacteria: Except for the Mg^{2+}-free experiments, the bacterial culture media were prepared with 10 mM $MgCl_2$ to ensure DNA origami stability. For this, 2.5 g LB (*B. subtilis* and *E. coli,* Carl-Roth) or TSB (*S. capitis*, MP Biomedicals) broth and 0.2033 g $MgCl_2{\cdot}6H_2O$ (≥99%, Carl-Roth) were dissolved in 100 mL molecular biology-grade water (VWR) and autoclaved at 121 °C for 15 min. Then, 500 µL of each bacterial stock (*B. subtilis*, DSM 5545, *S. capitis* subsp. *urealyticus*, DSM 6717, and *E. coli*, DSM 5695) were inoculated into 40 mL medium and incubated overnight at 37 °C in a shaking incubator at 150 rpm. Afterward, 500 µL of the overnight suspension was added to 40 mL medium and incubated at 37 °C and 150 rpm until the culture reached the logarithmic phase.

Enzyme-linked oligonucleotide assay (ELONA): For ELONA, six edge staples of the DON triangle were replaced with biotinylated sequences (see Figure S21 and table S2, Supporting Information). After DON assembly, the 1x TAE buffer was exchanged against PBS with 10 mM $MgCl_2$ during spin filtering. *B. subtilis* (DSM 5545), *S. capitis* (DSM 6717), and *E. coli* (DSM 5695) were diluted in PBS (pH 7.4, Sigma-Aldrich) to OD600 = 0.5. Afterward, 100 µL of the bacteria samples were deposited in the designated wells of a 96-well plate (Nunc-Immuno MaxiSorp MicroWell 96 well solid plate, Sigma-Aldrich), and incubated at 4 °C overnight. Afterward, the wells were washed three times with 200 µL of PBS supplemented with 0.05% Tween 20. Subsequently, 100 µL V36–DONs, V18–DONs, and bare DONs at 46 nM in PBS with 10 mM $MgCl_2$ were added to the designated wells and incubated at room temperature for 1 h. Afterward, the wells were washed three times with PBS supplemented with 0.02% Tween 20 and incubated with 100 µL of 125 ng mL^{-1} HRP-conjugated streptavidin (1.25 mg mL^{-1}, Thermo Fisher) at room temperature for 1 h. After incubation, the wells were washed five times with PBS. Finally, the wells were incubated with 100 µL of TMB substrate solution (1-Step Ultra TMB-ELISA Substrate Solution, Thermo Fisher) at room temperature for 15 min, after which the reaction was stopped by adding 50 µL of 1 M H_2SO_4 (96% Stockmeier Chemie) solution. The optical density at 450 nm was recorded with a plate reader Tristar2 S LB 942 (Berthold Technologies).

Inhibition assay: *B. subtilis* (DSM 5545) was grown overnight at 37 °C at 150 rpm in an incubator 222DS (Labnet). Afterward, the bacteria were inoculated in 15 mL of LB medium (Carl Roth) and allowed to grow until the OD600 reached a value of 0.3. Serial dilutions of nonmodified vancomycin and V36–DONs in 50 µl 2x TAE containing 10 mM $MgCl_2$ were performed in a 96-well plate. Following this, 50 µL of *B. subtilis* bacterial culture at OD600 = 0.3 was added to each well, leading to a final vancomycin concentration of 2.91 µM in the first well and 0.091 µM in the last well at a final volume of 100 µL. The OD600 values were measured after 0 h and 24 h incubation at 37 °C using a Tristar2 S LB 942 (Berthold Technologies) to monitor the bacterial growth. A single vancomycin-conjugated staple was tested as well at a single concentration of 2.91 µM. Both nonmodified vancomycin and V36–DONs were also tested against *S. capitis* and *E. coli* at the same vancomycin concentration using the same protocol.

Scanning Electron Microscopy (SEM): Silicon wafers were cleaned in RCA-1 solution (1:1:5 v/v of 35% NH_4OH, 25% H_2O_2, and H_2O) at 75 °C for 15 min. After cleaning, the wafers were rinsed with HPLC-grade water and dried using argon gas. Subsequently, the wafers were incubated with 1 mL of 0.01% w/v poly-L-lysine (Sigma-Aldrich) solution for 2 h at room temperature in the dark. Following incubation, the wafers were rinsed with HPLC-grade water, dried with argon gas, and stored at 4 °C in the dark. *B. subtilis* was grown and incubated with free vancomycin and V36–DON under the same conditions as described for the inhibition assay. Both compounds were prepared in 2x TAE buffer containing 10 mM $MgCl_2$ at a final concentration of 2.91 µM and incubated with *B. subtilis* culture (OD600 = 0.3) for 4 h at 37 °C in a 24-well plate. Following this incubation, silicon wafers were added to the mixture and further incubated for 2 h at 37 °C. To prepare the samples for SEM imaging, the wafers were immersed in 3% glutaraldehyde (Sigma-Aldrich) dissolved in PBS for 24 h at 4 °C. Subsequently, the wafers were washed with PBS and dehydrated by sequential immersion in ethanol solutions of 20%, 40%, 60%, 80%, and 100% v/v for 20 min each. After dehydration, the samples were stored at 4 °C. For SEM imaging, the sample surfaces were sputter-coated (SCD 500, Leica Microsystems) with a 3 nm gold alloy film (80% Au and 20% Pd) and examined using a Zeiss NEON 40 SEM at a beam energy of 5 kV.

Statistical analysis: Experiments were performed in triplicates (n = 3) and are presented as the mean ± standard deviation. Statistical significance was determined by calculating p values using either a two-sided t-test in Excel (Figure 2d) or a one-way ANOVA in Origin (Figure 3a, 3b, and 4).

Supporting Information

Supporting Information is available from the Wiley Online Library or from the author.

Acknowledgements

This work was supported by Paderborn University via the Paderborn University Research Award 2022 (to A.K.). The authors acknowledge support for the publication cost by the Open Access Publication Fund of Paderborn University.

Conflict of Interest

The authors declare no conflict of interest.

Author Contributions

Özge Coskuner Leineweber: formal analysis (equal); investigation (equal); methodology (supporting); validation (equal); visualization (supporting); writing—original draft (supporting); writing—review and editing (equal). **Bhanu K. Pothineni**: conceptualization (supporting); formal analysis (equal); methodology (supporting); validation (equal); visualization (equal); writing—original draft (supporting); writing—review and editing (equal). **Nils Schumann**: formal analysis (supporting); investigation (supporting); writing—review and editing (equal). **Ulrike Hofmann**: formal analysis (supporting); investigation (equal); writing—review and editing (equal). **Christin Möser**: investigation (supporting); methodology (supporting); writing—review and editing (equal). **David M. Smith**: conceptualization (supporting); methodology (supporting); supervision (supporting); writing—review and editing (equal). **Guido Grundmeier**: resources (equal); supervision (supporting); writing—review and editing (equal). **Yixin Zhang**: conceptualization (equal); methodology (equal); resources (equal); supervision (equal); writing—review and editing (equal). **Adrian Keller**: conceptualization (equal); formal analysis (supporting); funding acquisition (lead); methodology (equal); supervision (equal); visualization (supporting); writing—original draft (lead); writing—review and editing (equal). **Özge Coskuner Leineweber** and **Bhanu K. Pothineni** contributed equally to this work.

Data Availability Statement

The data that support the findings of this study are available in the supplementary material of this article.

Keywords

Bacillus subtilis, DNA origami, *Escherichia coli*, glycopeptide antibiotics, *Staphylococcus capitis*

Received: April 16, 2025
Revised: July 15, 2025
Published online:

[1] M. Naghavi, S. E. Vollset, K. S. Ikuta, L. R. Swetschinski, A. P. Gray, E. E. Wool, G. Robles Aguilar, T. Mestrovic, G. Smith, C. Han, R. L. Hsu, J. Chalek, D. T. Araki, E. Chung, C. Raggi, A. Gershberg Hayoon, N. Davis Weaver, P. A. Lindstedt, A. E. Smith, U. Altay, N. V. Bhattacharjee, K. Giannakis, F. Fell, B. McManigal, N. Ekapirat, J. A. Mendes, T. Runghien, O. Srimokla, A. Abdelkader, S. Abd-Elsalam, et al.,*Lancet* **2024**, *404*, 1199.
[2] Wanted: a reward for antibiotic development, *Nat. Biotechnol.* **2018**, *36*, 555.
[3] M. A. Cooper, D. Shlaes, *Nature* **2011**, *472*, 32.
[4] M. Balasegaram, K. Outterson, J.-A. Røttingen, *Lancet* **2024**, *404*, 1385.
[5] R. Laxminarayan, A. Duse, C. Wattal, A. K. M. Zaidi, H. F. L. Wertheim, N. Sumpradit, E. Vlieghe, G. L. Hara, I. M. Gould, H. Goossens, C. Greko, A. D. So, M. Bigdeli, G. Tomson, W. Woodhouse, E. Ombaka, A. Q. Peralta, F. N. Qamar, F. Mir, S. Kariuki, Z. A. Bhutta, A. Coates, R. Bergstrom, G. D. Wright, E. D. Brown, O. Cars, *Lancet Infect. Dis.* **2013**, *13*, 1057.
[6] R. Lakshminarayanan, E. Ye, D. J. Young, Z. Li, X. J. Loh, *Adv. Healthcare Mater.* **2018**, *7*, e1701400.
[7] J. Ndayishimiye, T. Kumeria, A. Popat, J. R. Falconer, M. A. T. Blaskovich, *ACS Infect. Dis.* **2022**, *8*, 693.
[8] B. K. Pothineni, A. Keller, *Adv. Nanobiomed Res.* **2023**, *3*, 2200134.
[9] Y.-C. Yeh, T.-H. Huang, S.-C. Yang, C.-C. Chen, J.-Y. Fang, *Front. Chem.* **2020**, *8*, 286.
[10] D. M. Smith, A. Keller, *Adv. Nanobiomed Res.* **2021**, *1*, 2000049.
[11] P. W. K. Rothemund, *Nature* **2006**, *440*, 297.
[12] E.-C. Wamhoff, G. A. Knappe, A. A. Burds, R. R. Du, B. W. Neun, S. Difilippantonio, C. Sanders, E. F. Edmondson, J. L. Matta, M. A. Dobrovolskaia, M. Bathe, *ACS Appl. Bio Mater.* **2023**, *6*, 1960.
[13] C. R. Lucas, P. D. Halley, A. A. Chowdury, B. K. Harrington, L. Beaver, R. Lapalombella, A. J. Johnson, E. K. Hertlein, M. A. Phelps, J. C. Byrd, C. E. Castro, *Small* **2022**, *18*, e2108063.
[14] F. Praetorius, B. Kick, K. L. Behler, M. N. Honemann, D. Weuster-Botz, H. Dietz, *Nature* **2017**, *552*, 84.
[15] C. Chau, G. Mohanan, I. Macaulay, P. Actis, C. Wälti, *Small* **2024**, *20*, e2308776.
[16] Y. Xin, P. Piskunen, A. Suma, C. Li, H. Ijäs, S. Ojasalo, I. Seitz, M. A. Kostiainen, G. Grundmeier, V. Linko, A. Keller, *Small* **2022**, *18*, e2107393.
[17] S. Ramakrishnan, B. Shen, M. A. Kostiainen, G. Grundmeier, A. Keller, V. Linko, *ChemBioChem* **2019**, *20*, 2818.
[18] H. J. Rodríguez-Franco, P. B. M. Hendrickx, M. M. C. Bastings, *ACS Polym. Au* **2025**, *5*, 35.
[19] I. Seitz, H. Ijäs, V. Linko, M. A. Kostiainen, *ACS Appl. Mater. Interfaces* **2022**, *14*, 38515.
[20] F. Kollmann, S. Ramakrishnan, B. Shen, G. Grundmeier, M. A. Kostiainen, V. Linko, A. Keller, *ACS Omega* **2018**, *3*, 9441.
[21] H. Ijäs, B. Shen, A. Heuer-Jungemann, A. Keller, M. A. Kostiainen, T. Liedl, J. A. Ihalainen, V. Linko, *Nucleic Acids Res.* **2021**, *49*, 3048.
[22] N. Navarro, A. Aviñó, Ò. Domènech, J. H. Borrell, R. Eritja, C. Fàbrega, *Nanomedicine* **2024**, *55*, 102722.
[23] I. Mela, P. P. Vallejo-Ramirez, S. Makarchuk, G. Christie, D. Bailey, R. M. Henderson, H. Sugiyama, M. Endo, C. F. Kaminski, *Angew. Chem. Int. Ed. Engl.* **2020**, *59*, 12698.
[24] J. Liu, L. Song, S. Liu, Q. Jiang, Q. Liu, N. Li, Z.-G. Wang, B. Ding, *Nano Lett.* **2018**, *18*, 3328.
[25] M. Hanke, G. Grundmeier, A. Keller, *Nanoscale* **2022**, *14*, 11552.
[26] Y. Zhang, X. Tian, Z. Wang, H. Wang, F. Liu, Q. Long, S. Jiang, *Front. Mol. Biosci.* **2023**, *10*, 1239952.
[27] S. Zhang, X.-Y. Lou, L. Liu, Y.-W. Yang, *Adv. Healthcare Mater.* **2023**, *12*, e2301066.
[28] T. Wu, H. Wang, R. Tian, S. Guo, Y. Liao, J. Liu, B. Ding, *Angew. Chem. Int. Ed. Engl.* **2023**, *62*, e202311698.
[29] L. Rabbe, J. A. Garcia-Diosa, G. Grundmeier, A. Keller, *Small Struct.* **2024**, *5*, 2400094.
[30] Y. Ahmadi, T. R. Umrekar, N. Mutter, M. Beeby, I. Barišić, *Biosens. Bioelectron. X* **2024**, *16*, 100436.
[31] Y. Sakai, M. S. Islam, M. Adamiak, S. C.-C. Shiu, J. A. Tanner, J. G. Heddle, *Genes* **2018**, *9*, 571.
[32] F. Bottari, E. Daems, A.-M. de Vries, P. van Wielendaele, S. Trashin, R. Blust, F. Sobott, A. Madder, J. C. Martins, K. de Wael, *J. Am. Chem. Soc.* **2020**, *142*, 19622.
[33] C. Bayraç, H. A. Öktem, *J. Mol. Recognit.* **2017**, *30*, e2583.
[34] T. Hianik, V. Ostatná, M. Sonlajtnerova, I. Grman, *Bioelectrochemistry* **2007**, *70*, 127.
[35] V. Ostatná, H. Vaisocherová, J. Homola, T. Hianik, *Anal. Bioanal. Chem.* **2008**, *391*, 1861.
[36] J.-G. Walter, O. Kökpinar, K. Friehs, F. Stahl, T. Scheper, *Anal. Chem.* **2008**, *80*, 7372.
[37] C. Da Pieve, P. Williams, D. M. Haddleton, R. M. J. Palmer, S. Missailidis, *Bioconjug. Chem.* **2010**, *21*, 169.
[38] Y. Ahmadi, R. Soldo, K. Rathammer, L. Eibler, I. Barišić, *Anal. Chem.* **2021**, *93*, 5161.
[39] M. G. Córdova-Espinoza, R. González-Vázquez, R. R. Barron-Fattel, R. Gónzalez-Vázquez, M. A. Vargas-Hernández, E. M. Albores-Méndez, A. L. Esquivel-Campos, F. Mendoza-Pérez, L. Mayorga-Reyes, M. A. Gutiérrez-Nava, K. Medina-Quero, A. Escamilla-Gutiérrez, *Int. J. Mol. Sci.* **2024**, *25*, 1257.
[40] E. Rubinstein, Y. Keynan, *Front. Public Health* **2014**, *2*, 217.
[41] J. Rao, J. Lahiri, L. Isaacs, R. M. Weis, G. M. Whitesides, *Science* **1998**, *280*, 708.
[42] A. J. Kell, G. Stewart, S. Ryan, R. Peytavi, M. Boissinot, A. Huletsky, M. G. Bergeron, B. Simard, *ACS Nano* **2008**, *2*, 1777.
[43] S. Lin, Y. Zheng, Y. Xing, K. Dou, R. Wang, H. Cui, F. Yu, *Talanta* **2024**, *280*, 126691.
[44] X. Meng, G. Yang, F. Li, T. Liang, W. Lai, H. Xu, *ACS Appl. Mater. Interfaces* **2017**, *9*, 21464.
[45] M. Rashid, M. A. Rabbi, T. Ara, M. M. Hossain, M. S. Islam, A. Elaissari, H. Ahmad, M. M. Rahman, *RSC Adv.* **2021**, *11*, 36319.
[46] C. Zhang, C. Wang, R. Xiao, L. Tang, J. Huang, Di Wu, S. Liu, Y. Wang, D. Zhang, S. Wang, X. Chen, *J. Mater. Chem. B* **2018**, *6*, 3751.
[47] M. Sample, H. Liu, T. Diep, M. Matthies, P. Šulc, *ACS Nano* **2024**, *18*, 30004.
[48] S. Duhr, D. Braun, *Proc. Natl. Acad. Sci. U. S. A.* **2006**, *103*, 19678.
[49] A. Keller, J. Rackwitz, E. Cauët, J. Liévin, T. Körzdörfer, A. Rotaru, K. V. Gothelf, F. Besenbacher, I. Bald*Sci. Rep.* **2014**, *4*, 7391.
[50] C. Kielar, F. V. Reddavide, S. Tubbenhauer, M. Cui, X. Xu, G. Grundmeier, Y. Zhang, A. Keller, *Angew. Chem. Int. Ed. Engl.* **2018**, *57*, 14873.
[51] C. Kielar, S. Zhu, G. Grundmeier, A. Keller, *Angew. Chem. Int. Ed. Engl.* **2020**, *59*, 14336.
[52] A. Keller, I. Bald, A. Rotaru, E. Cauët, K. V. Gothelf, F. Besenbacher, *ACS Nano* **2012**, *6*, 4392.
[53] A. Keller, J. Kopyra, K. V. Gothelf, I. Bald, *New J. Phys.* **2013**, *15*, 83045.

[54] J. Huang, A. Suma, M. Cui, G. Grundmeier, V. Carnevale, Y. Zhang, C. Kielar, A. Keller, *Small Struct.* **2020**, *1*, 2000038.
[55] L. Rabbe, E. Tomm, G. Grundmeier, A. Keller, *RSC Adv.* **2025**, *15*, 24536.
[56] L. E. Hancock, B. E. Murray, J. Sillanpää, *Enterococci: From Commensals To Leading Causes Of Drug Resistant Infection* (Eds: M. S. Gilmore, D. B. Clewell, Y. Ike, N. Shankar), Massachusetts Eye and Ear Infirmary, Boston **2014**.
[57] I. Reviakine, D. Johannsmann, R. P. Richter, *Anal. Chem.* **2011**, *83*, 8838.
[58] S. Siddiqui, J. Yuan, *Molecules* **2021**, *26*, 204.
[59] D. Morzy, C. Tekin, V. Caroprese, R. Rubio-Sánchez, L. Di Michele, M. M. C. Bastings, *Nanoscale* **2023**, *15*, 2849.
[60] F. Ahimou, M. Paquot, P. Jacques, P. Thonart, P. G. Rouxhet, *J. Microbiol. Methods* **2001**, *45*, 119.
[61] C. Fang, E. Stiegeler, G. M. Cook, T. Mascher, S. Gebhard, *PLoS One* **2014**, *9*, e93169.
[62] P. Bisicchia, N. K. Bui, C. Aldridge, W. Vollmer, K. M. Devine, *Mol. Microbiol.* **2011**, *81*, 157.
[63] D. M. Angeles, D.-J. Scheffers, *Curr. Issues Mol. Biol.* **2021**, *41*, 539.
[64] A. Suma, A. Stopar, A. W. Nicholson, M. Castronovo, V. Carnevale, *Nucleic Acids Res.* **2020**, *48*, 4672.
[65] M. Hanke, E. Tomm, G. Grundmeier, A. Keller, *ChemBioChem* **2023**, *24*, e202300338.
[66] Y. Xin, X. Ji, G. Grundmeier, A. Keller, *Nanoscale* **2020**, *12*, 9733.
[67] D. M. Crepin, M. Chavignon, P. O. Verhoeven, F. Laurent, J. Josse, M. Butin, *Clin. Microbiol. Rev.* **2024**, *37*, e0011823.
[68] T. Lavoie, K. E. Daffinee, M. L. Vicent, K. L. LaPlante, *Microbiol. Spectr.* **2025**, *13*, e0291524.
[69] M. Bonten, J. R. Johnson, A. H. J. van den Biggelaar, L. Georgalis, J. Geurtsen, P. I. de Palacios, S. Gravenstein, T. Verstraeten, P. Hermans, J. T. Poolman, *Clin. Infect. Dis.* **2021**, *72*, 1211.
[70] J. B. Kaper, J. P. Nataro, H. L. Mobley, *Nat. Rev. Microbiol.* **2004**, *2*, 123.
[71] C. J. L. Murray, K. S. Ikuta, F. Sharara, L. Swetschinski, G. Robles Aguilar, A. Gray, C. Han, C. Bisignano, P. Rao, E. Wool, S. C. Johnson, A. J. Browne, M. G. Chipeta, F. Fell, S. Hackett, G. Haines-Woodhouse, B. H. Kashef Hamadani, E. A. P. Kumaran, B. McManigal, S. Achalapong, R. Agarwal, S. Akech, S. Albertson, J. Amuasi, J. Andrews, A. Aravkin, E. Ashley, F.-X. Babin, F. Bailey, S. Baker, et al., *Lancet* **2022**, *399*, 629.
[72] A. Gyurova, V. Doltchinkova, R. Georgieva, S. Danova, S. Stoylov, *Open Chem.* **2013**, *11*, 801.
[73] V. Yarlagadda, G. B. Manjunath, P. Sarkar, P. Akkapeddi, K. Paramanandham, B. R. Shome, R. Ravikumar, J. Haldar, *ACS Infect. Dis.* **2016**, *2*, 132.
[74] V. Linko, A. Keller, *Small* **2023**, *19*, e2301935.
[75] J. García-Fernández, L. Rivadulla Costa, C. Pinto-Díez, M. Elena Martín, V. M. González, M. de La Fuente Freire, *Nanoscale* **2023**, *15*, 19110.
[76] K. Yamagishi, K. Sawaki, A. Murata, S. Takeoka, *Chem. Commun.* **2015**, *51*, 7879.
[77] K. Barker, S. K. Rastogi, J. Dominguez, T. Cantu, W. Brittain, J. Irvin, T. Betancourt, *J. Biomater. Sci. Polym. Ed.* **2016**, *27*, 22.
[78] B. K. Pothineni, G. Grundmeier, A. Keller, *Nanoscale* **2023**, *15*, 12894.
[79] D. Nečas, P. Klapetek, *Open Phys.* **2012**, *10*, 181.